ISSN 0029-3865

CNPq

CBPF- CENTRO BRASILEIRO DE PESQUISAS FÍSICAS

Notas de Física

CBPF-NF-007/94

January 1994

Electric-Field Gradients and Magnetic Hyperfine Parameters of Square-Pyramidal $[M(CN)_5]^{3-}$(M=Co, Rh and Ir) Complexes

S.R. Nogueira* and Diana Guenzburger

Centro Brasileiro de Pesquisas Físicas, Rua Dr. Xavier Sigaud, 150, 22290-180, Rio de Janeiro/RJ, Brasil

*Instituto de Física, Universidade Federal do Rio de Janeiro, Cidade Universitária, Ilha do Fundão, 21945-970, Rio de Janeiro/RJ, Brazil

Abstract

Density functional self-consistent spin-polarized calculations with the Discrete Variational method were performed to obtain the electronic structure of the paramagnetic complexes $[Co(CN)_5]^{3-}$, $[Rh(CN)_5]^{3-}$ and $[Ir(CN)_5]^{3-}$ of square-pyramidal geometry. All electrons were kept in the variational space. Electric field gradients and magnetic hyperfine parameters at the metal site were computed with the molecular charge and spin densities obtained and compared with experimental values derived by Electron Paramagnetic Resonance. It was found that the Fermi interaction is critically dependent on the angle between the axial and equatorial CN ligands.

Key-words: Hyperfine parameters; Transition metal complexes.

1 Introduction

The diamagnetic complex ions $[M(CN)_6]^{n-}$, where M is a transition metal, may be inserted in crystalline hosts such as NaCl, KCl, etc; after irradiation with X-rays or 2MeV electrons, several reduced paramagnetic species may be obtained, some in unusual geometries and/or oxidation states of the metal [1]. Such is the case of $[M(CN)_5]^{3-}$(M=Co, Rh and Ir), where M has formal charge +2, obtained in solid matrices by irradiation of the diamagnetic complexes $[M(CN)_6]^{3-}$ of octahedral symmetry, which lose one ligand in the process. The pentacoordinated species are covalent paramagnetic complexes and their investigation by Electron Paramagnetic Resonance (EPR) allows the examination of the metal-CN bond with this technique.

The study of EPR spectra, with the aid of the effective spin Hamiltonian, may give valuable insight on the geometry and chemical bond of a given molecule or ion. However, the microscopic origin of the spin Hamiltonian parameters obtained from the fit to the spectra may only be fully understood with the aid of accurate quantum chemical calculations. With this purpose, we have performed electronic structure calculations for the complex ions $[Co(CN)_5]^{3-}$, $[Rh(CN)_5]^{3-}$ and $[Ir(CN)_5]^{3-}$. The hyperfine parameters of the spin Hamiltonian were obtained, with the use of second-order perturbation theory [2, 3] and compared to experimental results when available. The calculated values were analysed in terms of the electronic charge and spin distributions.

The method employed was the Discrete Variational (DV) [4], in the framework of Density Functional Theory [5]. Methods based in this theory have been proved useful in deriving properties of transition metal molecules and complex ions [6]; in spite of being less demanding computationally, they often give results that are more accurate than those obtained with Hartree-Fock-based methods. Moreover, electron correlation effects are included, while retaining the simplicity of a single-particle description.

This report is organized as follows: in section II the theoretical method is briefly described; in section III are given details of the electronic structure; in section IV the results for the electric field gradients are presented; in section V the magnetic hyperfine parameters are derived, and in section VI we summarize our conclusions.

2 Theoretical Method

The DV method has been described in detail elsewhere [4]; here we give a summary of its main aspects and specific features pertaining to the present calculations. With the DV method one solves the set of one-electron Kohn-Sham equations [7] of density functional theory [5] in the local-density approximation (in hartree atomic units):

$$[-1/2\nabla^2 + V_c(\vec{r}) + V_{xc}^{\sigma}(\vec{r})]\phi_{i\sigma}(\vec{r}) = \varepsilon_{i\sigma}(\vec{r}). \quad (1)$$

In eqs. (1), the Coulomb potential V_c includes electron-nucleus and electron-electron interactions, and V_{xc}^{σ} is the exchange-correlation potential of spin σ. We employed V_{xc}^{σ} as derived by von Barth and Hedin [8]. In the present spin-polarized calculations, the molecular orbitals $\phi_{i\sigma}$ are allowed to be different for each spin σ. The molecular potentials are functions of the electron density ρ_{σ} of spin σ.

$$\rho_{\sigma}(\vec{r}) = \sum_i n_{i\sigma}|\phi_{i\sigma}(\vec{r})|^2 \quad (2)$$

where $n_{i\sigma}$ is the occupation of molecular orbital $\phi_{i\sigma}$. These latter are expanded as linear combinations of numerical atomic orbitals χ_μ

$$\phi_{i\sigma}(\vec{r}) = \sum_\mu \chi_\mu(\vec{r}) C^\mu_{i\sigma} \tag{3}$$

obtained by atomic self-consistent-field local density calculations. By minimization of the error functionals associated with each orbital $\phi_{i\sigma}$ in a three-dimensional grid of points, the secular equations are obtained

$$[\mathrm{H}][\mathrm{C}] = [\mathrm{E}][\mathrm{S}][\mathrm{C}] \tag{4}$$

in which the matrix elements are summations over the 3-dimensional grid of points. These equations, in which [H] is the hamiltonian matrix and [S] the overlap matrix, are solved self-consistently until a desired criterion is met. Here the convergence was carried up to a difference of $\leq 10^{-3}$ in the charge and spin densities.

To facilitate the computation of the electron-electron repulsion integrals, the molecular charge density was fitted to a multipolar expansion [9] with variational coefficients d_j:

$$\rho(\vec{r}) \cong \sum_j d_j \rho_j(\vec{r}) \tag{5}$$

where

$$\rho_j(\vec{r}) = \sum_\nu{}' \sum_m C^{\nu\lambda}_{\ell m} R_N(r_\nu) Y^m_\ell(\hat{r}_\nu) \tag{6}$$

In Eq. (6), j are atoms of a set I equivalent by symmetry, R_N are radial functions centered at atoms ν, and λ is a basis function associated to a particular value of ℓ. The prime in the first summation indicates the restriction to atoms in the set I. In the present calculations, partial waves up to $\ell = 2$ were included for all atoms, giving a maximum least-squares error in the fit of ρ of 0.03.

The basis set employed here includes the valence nd, (n+1)s and (n+1)p orbitals of the transition element; all core orbitals of all atoms were kept in the variational space, i.e., no "frozen core" approximation was employed. The basis functions were improved, after convergence with a given set, obtaining a new basis by performing calculations for atoms with the configuration obtained in the molecular complexes. The atomic configurations were derived by a Mulliken-type population analysis [10, 11] in which the overlap population is divided proportional to the coefficient of the atom in the molecular orbital.

The 3-dimensional grid employed was divided in two regions. Around the nucleus of the transition metal is placed a sphere, where a precise polinomial integration is performed over a regular grid [12]; outside this sphere, the points are generated by the pseudo-random Diophantine method [4]. The number of points employed in the present calculations were 4000 inside the sphere and 6500 for the rest of the molecular complex volume. This scheme assures the necessary numerical precision, in particular at the core region of the transition element where the wave functions oscilate severely.

3 Electronic Structure

It has been determined experimentally that the pentacyano complexes studied here have square-pyramidal geometries, with point group C_{4v} [1]. In Fig. 1 is depicted $[Co(CN)_5]^{3-}$; $[Rh(CN)_5]^{3-}$ and $[Ir(CN)_5]^{3-}$ are expected to have similar structures. The fact that the metal lies above the equatorial plane is evidenced by EPR measurements of the super-hyperfine interaction on the equatorial nitrogens [13]. Furthermore, X-rays diffraction of single crystals of $[NEt_2(i\text{-}Pr)_2]_3$ $[Co(CN)_5]$ [14] and $[Cr(NH_3)_6][Ni(CN)_5].2H_2O$ [15] gives for the $(CN)_{ax}$-M-$(CN)_{eq}$ angle Θ (see Fig. 1) the values 97.7^0 and 100.2^0, respectively. We have thus performed calculations for three angles, 95^0, 97.7^0 and 101^0, for all three complexes. In all calculations the C-N interatomic distance considered was $1.15\mathring{A}$. The Co-C distances were made equal to the experimental values [14]: Co-C_{ax}=$2.01\mathring{A}$ and Co-C_{eq}=$1.89\mathring{A}$. The interatomic distances Rh-C_{ax}=Rh-C_{eq}=$1.98\mathring{A}$ and Ir-C_{ax}=Ir-C_{eq}=$2.00\mathring{A}$, not experimentally available, were estimated by extrapolating values determined for hexacyano complexes [16].

In Fig. 2 are depicted the one-electron valence energy levels (eigenvalues $\varepsilon_{i\sigma}$ of Eq. 1) for the three complexes studied. Although these energies may not strictly be compared to molecular orbital energies in the sense of Hartree-Fock, since in local density theory Koopman's theorem does not hold [17], this may be done approximatly. The strongly covalent nature of the M-CN bond assures a low-spin configuration, with the unpaired electron occupying orbitals of a_1 symmetry. The $^2A_1$ ground state found for all three complexes is in accord with EPR measurements. The "crystal field" levels, i.e., antibonding orbitals strongly localized on the metal, are $2b_2$, 11e, $17a_1$ (occupied) and $7b_1$ (virtual) for $[Co(CN)_5]^{3-}$. These levels have a large contribution from Co(3d) and are derived from the σ levels e_g (a_1 and b_1) and the π levels t_{2g} (b_2 and e) of octahedral symmetry. The fact that the antibonding a_1 orbital has a much lower energy than its b_1 counterpart in all three cases derives from the absence of the sixth ligand (see Fig. 1), that weakens the bond along the z axis involving the orbitals of a_1 symmetry. All the valence levels of lower energy are mainly localized on N(2p), C(2s) and C(2p). The molecular orbitals derived from N(2s), of deeper energies, are not shown in the figure.

The valence molecular orbital schemes for $[Rh(CN)_5]^{3-}$ and $[Ir(CN)_5]^{3-}$ have a similar structure. Some differences are noticed, however. First, the admixture of the ligand functions with the metal in the bonding orbitals is higher than in $[Co(CN)_5]^{3-}$, particularly in the orbitals $5b_1$-9e of $[Rh(CN)_5]^{3-}$, and $19a_1$-13e of $[Ir(CN)_5]^{3-}$. The occupied "crystal field" levels of $[Rh(CN)_5]^{3-}$ i.e., levels with large contribution from Rh(4d), are $3b_2$, 13e and $20a_1$, analogous to $[Co(CN)_5]^{3-}$. However, unlike $[Co(CN)_5]^{3-}$, the 4d character in the virtual orbitals is distributed among $8b_1$ (~30% 4d) and $9b_1$ (~20% 4d). This feature is even more pronounced in $[Ir(CN)_5]^{3-}$: the occupied "crystal field" levels are $5b_2$, 17e and $24a_1$, but the 5d participation in the lowest-energy level of b_1 symmetry ($10b_1$) is only ~4%, whereas $11b_1$ has ~42% Ir(5d) character.

The order of the crystal field levels b_2<e found in all three cases has been obtained in a semiempirical calculation for $[Co(CN)_5]^{3-}$ [18], and is a consequence of the metal being above the equatorial plane of the ligands.

Another noticeable feature in the molecular orbitals schemes of the three complexes is the much smaller energy difference between the crystal field levels ($2b_2$, 11e) and $17a_1$, as well as between $17a_1$ and $7b_1$ in $[Co(CN)_5]^{3-}$, as compared to the corresponding energy

differences in the Rh and Ir complexes. In other words, a larger "crystal field splitting" occurs for the heavier metals. This is coherent with the optical spectra of the hexacyano complexes $[Rh(CN)_6]^{3-}$ and $[Ir(CN)_6]^{3-}$, that show d→d transitions occurring at higher energies than $[Co(CN)_6]^{3-}$, being obscured by charge-transfer bands of high intensity [19, 20]. The proximity of the $17a_1$ orbital containing the unpaired electron in $[Co(CN)_5]^{3-}$ to the other occupied levels explains the larger spin splittings observed, as compared to the Rh and Ir complexes.

In Table I are displayed the charges, Mulliken-type populations, magnetic moments and distribution of the unpaired electron in the HOMO ($17a_1\uparrow$ in $[Co(CN)_5]^{3-}$, $20a_1\uparrow$ in $[Rh(CN)_5]^{3-}$ and $24a_1\uparrow$ in $[Ir(CN)_5]^{3-}$), for $\Theta = 97.7^0$. Magnetic moments are defined as the difference between spin up and spin down populations. The calculations for the other values of Θ (95^0 and 101^0) show very small differences from the values for 97.7^0; however, in some cases these small differences have a large effect in the hyperfine interactions, as shall be seen futher on.

From Table I it is verified that the charge on the transition metal is much smaller than the formal value +2. The 5d population is somewhat smaller in $[Ir(CN)_5]^{3-}$, and so the Ir charge is larger. The negative charge on the CN ligands is polarized towards the nitrogens.

The total magnetic moments are constituted mainly of metal nd. The axial C, however, shows a significant contribution and the axial N a small antiferromagnetic coupling. The magnetic moments on the equatorial C and N atoms are very small. Thus we conclude that the spin of the molecular complexes is distributed mainly along the z axis. In comparing the three complexes, one notices a significant reduction of the nd contribution to the total magnetic moments in the order Co>Rh>Ir, followed by an increase in (n+1)p and in the ligands participation. Therefore, the spin is more delocalized for the heavier transition metal complexes.

The total magnetic moment may be divided in two contributions: that from the unpaired electron in the HOMO, and that which arises from the polarization of the closed shells by the unpaired electron. Comparison of the total magnetic moments with the distribution of the unpaired electron in the HOMO shows that the total contribution of the metal arises almost solely from the unpaired electron in $[Rh(CN)_5]^{3-}$ and $[Ir(CN)_5]^{3-}$; in contrast, for $[Co(CN)_5]^{3-}$ the total moment on Co is significantly higher than the HOMO contribution, evidencing a larger spin-polarization of the doubly-filled orbitals. This is coherent with the larger spin-splitting of the energy levels (Fig. 1) in $[Co(CN)_5]^{3-}$, as described earlier.

The nd character of the unpaired electron decreases in the order Co>Rh>Ir; this is followed by an increase in (n+1)p in the same order, such that the total metal contribution is almost constant, and by an increase in the contribution of the ligands.

4 Electric Field Gradients

The contribution of the electric quadrupole interaction to the spin Hamiltonian is [2]

$$H_Q = I.\tilde{P}.I \tag{7}$$

where I is the nuclear spin and $\tilde{P}$ the quadrupolar tensor with components given by

$$P_{\mu\nu} = \frac{eQ}{2I(2I-1)} V_{\mu\nu} \tag{8}$$

where Q is the quadrupole moment of the nucleus and $V_{\mu\nu}$ a component of the electric field gradient tensor. For the present complexes of axial symmetry, the tensor is diagonal, with $V_{zz} = -2V_{xx(yy)}$ denominated the electric field gradient by convention. This is given by, taking into account Eq. (2) [21],

$$V_{zz} = -\int \rho(\vec{r})(3z^2 - r^2)/r^5 d\vec{r} + \sum_q Z_q(3z_q^2 - r_q^2)/r_q^5 \tag{9}$$

The first term in Eq. (9) is the electronic contribution, calculated in the DV method as a sum over the 3-dimensional grid, and the second is the point-charge contribution of the surrounding C and N nuclei.

In Table II are given the calculated values of V_{zz} for $\Theta = 97.7^0$. In the first column are displayed the values for the "shallow core" of the transition metal (molecular orbitals with large contributions of Co(3s,3p), Rh(4s,4p) or Ir(5s,5p)). The contributions of the deeper core of the metals were also calculated, but were seen to be negligible due to the sphericity of these orbitals. The "shallow core" contributions are much smaller than the valence, and have opposite sign. They represent the distortion of the inner shells in reaction to the valence, which is often treated in an "ad hoc" manner with the use of atomic Sternheimer shielding factors [22]. In all three cases, the valence component is the largest. Calculations were also performed for the angles $\Theta = 95^0$ and 101^0, but the results differ insignificantly from $\Theta = 97.7^0$. It may be seen in Table II that the total V_{zz} is positive and increases strongly in the order Co<Rh<Ir.

Experimental values for comparison are only available for $[Ir(CN)_5]^{3-}$; these were obtained from EPR measurements of the component P_{zz} in Eq. (8), in solid NaCl, KCl and RbCl, and the sign was not determined [23]. The quadrupolar interaction may be observed experimentally in this case due to the large quadrupole moments of the ground states of ^{193}Ir (or ^{191}Ir), both with I=3/2. On the other hand, the isotope ^{103}Rh employed in EPR experiments has I=1/2 and thus no quadrupole moment in the ground state, making the determination of V_{zz} by EPR unviable. Our predicted value could be tested with the use of other techniques, possibly Time Differential Perturbed Angular Correlation (TDPAC) with the isotope ^{100}Rh. As for $[Co(CN)_5]^{3-}$, our predicted value for V_{zz} is very small; in fact, in spite of the significant value of Q of the ground state of ^{59}Co (+0.42b) [24], no quadrupole interaction is observed in EPR measurements [1, 25]. The experimental values of V_{zz} for $[Ir(CN)_5]^{3-}$ vary considerably with the host lattice; these do not contribute to V_{zz} due to their cubic symmetry. Since no such variation is observed theoretically when changing the angle Θ, we may only speculate that it must be the consequence of local lattice distortions and/or defect formation, which may be different in the different host crystals.

To investigate the mechanisms responsible for the sign and magnitude of the electric field gradient, we plotted in Table III the contributions to the valence V_{zz} of the molecular orbitals pertaining to the irreducible representations of the C_{4v} group. The results of two types of calculations are displayed: the calculations with all electrons in the variational space, and calculations in which all core orbitals were kept "frozen" in the metal, so that only nd, (n+1)s and (n+1)p were included in the SCF procedure. We observe significant differences between the results of the two procedures. Due to a small admixture of the "shallow core" p orbitals (Co(3p), Rh(4p) and Ir(5p)) in the valence MOs, the contributions of the irreducible representations a_1 and e (containing p_z and $p_{x(y)}$, respectively) are quite different in the two procedures. The effect of the "shallow core" orbitals mixture in the valence is amplified by their much larger values of $< r^{-3} >$, as may be observed in Table IV.

The values for the b_1 and b_2 symmetries almost do not change in the "frozen core" calculations, since they do not contain p orbitals; for a_1, the negative values are enhanced in the all-electron calculations, due to the negative contribution of the p_z orlbitals of the core. For the e symmetry, $d_{xz(yz)}$ contribute negatively and $p_{x(y)}$ positively [22]. When the core is relaxed, the $p_{x(y)}$ participation is enhanced, and the value becomes positive, or less negative; the effect is more pronounced than for a_1. The overall result of relaxing the core is much larger, positive values for V_{zz}. This is merely a reflexion of the "contraction" of the orbitals around the metal, due to the Pauli exclusion principle: this will be larger for the orbitals in the equatorial plane, with four ligands attached, than in the z axis, where a ligand is missing. The mixture with core orbitals will describe this contraction in the MO picture; a similar mechanism was observed in calculating V_{zz} for $[Au(CN)_2]^{1-}$ [26].

As for the increase in the total V_{zz} value in the order $[Co(CN)_5]^{3-}$ $<[Rh(CN)_5]^{3-}<[Ir(CN)_5]^{3-}$, it may be largely ascribed to increased values of $< r^{-3} >$ of the atomic orbitals of the metals along the series Co<Rh<Ir, as may be seen in Table IV. In fact, by considering the b_1 and b_2 irreducible representations where only nd orbitals are present and no ambiguity is possible we obtain $V_{zz}(b_1)(Co)/V_{zz}(b_1)(Rh) \approx < r^{-3} >$(Co 3d)/$< r^{-3} >$(Rh 4d) and $V_{zz}(b_1)(Rh)/V_{zz}(b_1)(Ir) \approx < r^{-3} >$(Rh 4d)/$< r^{-3} >$(Ir 5d).

5 Magnetic Hyperfine Interactions

In the spin Hamiltonian the magnetic hyperfine interactions are described by **[2, 3]:**

$$H_M = I.\tilde{A}.S \tag{10}$$

In the case of the present complexes, S=1/2. With the use of perturbation theory, we obtain the first-order components of the $\tilde{A}$ tensor, which are the Fermi (or contact) term A_F and dipolar terms $A_{\parallel}^D$ and $A_{\perp}^D$. A_F is defined as

$$A_F = \frac{8\pi}{3} g_e \mu_B g_N \mu_N [\rho_\uparrow(0) - \rho_\downarrow(0)] \tag{11}$$

where we made use of Eq. (2). g_e and g_N are the electronic and nuclear spectroscopic factors, respectively, μ_B the Bohr magneton and μ_N the nuclear magneton. In the present

C_{4v} symmetry, we have

$$\begin{aligned} A_{\parallel}^{D} &= A_{zz}^{D} = g_e \mu_B g_N \mu_N \int [\rho_\uparrow(\vec{r}) - \rho_\downarrow(\vec{r})](3z^2 - r^2)/r^5 d\vec{r} \\ A_{\perp}^{D} &= A_{x(y)}^{D} = -A_{\parallel}/2 \end{aligned} \tag{12}$$

In Eq. (12), the integral is calculated with the DV method as a sum over the 3-dimensional grid. For the $^2A_1$ ground state, the orbital contribution is zero in first order.

In the second order terms, only one-center terms centered on the metal were retained, due to the presence in the operators of r_M^{-3}. Furthermore, terms centered on C and N may be neglected due to the small spin-orbit constant of these atoms. Thus we have

$$A_{\parallel}^{(2)} = A_{zz}^{(2)} = (\pm) g_e \mu_B g_N \mu_N \sum_n{}' (E_0 - E_n)^{-1} [2 < \varphi_0 |\xi(r)\ell_z|\varphi_n >< \varphi_n |\ell_z/r^3|\varphi_0 > +$$
$$+ i < \varphi_0 |\xi(r)\ell_x|\varphi_n >< \varphi_n |3yz/r^5|\varphi_0 > - i < \varphi_0 |\xi(r)\ell_y|\varphi_n >< \varphi_n |3xz/r^5|\varphi_0 >] \tag{13}$$

where the prime on the second summation stands for restriction to the same spin in the excited states as in the ground state and all operators are centered on the transition metal. Only transitions from the occupied orbitals of e symmetry to the $a_1\downarrow$ ($\varphi_0\downarrow$) (–sign) and from $a_1\uparrow$ ($\varphi_0\uparrow$) to virtual levels of e symmetry (+sign) contribute, since the second-order perturbation involves mixture of excited states of A_2 and E symmetries with the ground state A_1. However, A_2 states were neglected since the a_2 orbitals do not have components on the metal. An analogous expression to Eq. (13) is employed for $A_{\perp}^{(2)}(=A_{xx(yy)})$. Spin-orbit constants were obtained by relativistic local-density atomic calculations [27], since $\xi_p = 2\Delta(\mathrm{p})/3$ for p orbitals, where $\Delta(\mathrm{p})$ is the energy splitting of the $p_{1/2}$ and $p_{3/2}$ levels; analogously, $\xi_d = 2\Delta(\mathrm{d})/5$ and $\xi_f = 2\Delta(\mathrm{f})/7$. Energy differences in Eq. (13) were obtained with transition state calculations [17] for the corresponding electronic transitions.

We have then for the total magnetic hyperfine tensor:

$$\begin{aligned} A_{\parallel} &= A_F + A_{\parallel}^{D} + A_{\parallel}^{(2)} \\ A_{\perp} &= A_F + A_{\perp}^{D} + A_{\perp}^{(2)} \end{aligned} \tag{14}$$

We may also recombine the terms in Eq. (14) such as to have isotropic (A_{ISO}) and anisotropic (A_{ANISO}) components:

$$\begin{aligned} A_{ISO} &= (A_{\parallel} + 2A_{\perp})/3 \\ A_{ANISO} &= (A_{\parallel} - A_{\perp})/3 \end{aligned} \tag{15}$$

The Fermi contribution is present only in A_{ISO} and the dipolar contribution only in A_{ANISO}.

In the calculation of A_F (Eq. (11)), the molecular orbitals were employed only for the valence electrons. For the core electrons, atomic local-density calculations were performed, for metal atoms in the same configuration as in the complex. This is due to the difficulty in polarizing the core with the LCAO basis functions employed. In non-relativistic theory, only molecular orbitals pertaining to the totally symmetric a_1 representation, containing ns functions, contribute to A_F.

In Table V are displayed the calculated components and total values of the magnetic hyperfine tensor at the Co site, for $[Co(CN)_5]^{3-}$. Experimental values obtained by EPR in several host crystals [25, 28] are given for comparison. We may see from the Table that the calculated values are critically dependent on the angle Θ. This dependence derives mainly from the A_F component, and from the positive contribution of the unpaired electron on the last occupied orbital of a_1 symmetry. In fact, as the angle Θ is increased, the 4s population in this orbital decreases and $3d_{z^2}$ increases, as may be seen in Fig. 3. This behavior of the populations in the HOMO is common to all three complexes, and may be understood as follows: as Θ increases, the Coulomb repulsion between the electronic charge in the diffuse 4s orbital and the equatorial CN ligands increases. Consequently, 4s charge is transferred into the more compact $3d_{z^2}$ orbital.

This dependence of A_F with Θ derived from the calculations explains the large variation observed in the measured values of A_{ISO} in different hosts (see Table V), and the relative insensitivity of A_{ANISO} to the environment. Different host crystals may induce small differences in Θ, and this will be reflected in A_F. As mentioned earlier, only A_{ISO} contains A_F.

In Table VI are shown the different contributions to $[\rho_\uparrow(0) - \rho_\downarrow(0)]$ in Eq. (11), at the transition metal site, for $[Co(CN)_5]^{3-}$ and $[Rh(CN)_5]^{3-}$. The core and valence contributions have different signs and almost cancel each other; the latter is almost entirely constituted of the HOMO $a_1\uparrow$ component, with a small contribution from the polarization of the valence closed shells.

It may be seen Table V that the theoretical values for $[Co(CN)_5]^{3-}$ for compare well with experiment, for Θ between 97.7^0 and 101^0.

In Table VII are displayed results for $[Rh(CN)_5]^{3-}$. A similar dependence with Θ is observed, due to the large sensitivity of A_F. As for experimental values, the only available data, obtained by EPR in NaCl host crystal, is $A_\perp < 5(10^{-4} cm^{-1})$ [29]; this is in accord with the theoretical values, particularly for Θ between 97.7^0 and 101^0. The much smaller magnitudes and reversed signs of all components of $[Rh(CN)_5]^{3-}$ as compared to $[Co(CN)_5]^{3-}$ are due to the g_N factors: $g_N(^{59}Co)$=+1.326 [30] and $g_N(^{103}Rh)$=−0.176 [30]. Actually, the electronic components of $A_{||}$ and $A_\perp$ are larger for $[Rh(CN)_5]^{3-}$.

As for $[Ir(CN)_5]^{3-}$, it was verified that the present perturbative treatment for $\tilde{A}$ is no longer accurate, due to the large spin-orbit constants of Ir. A relativistic theory of the hyperfine interactions would be indicated in this case, to obtain meaningful results.

6 Conclusions

Employing self-consistent spin-polarized density functional DV calculations for the paramagnetic complex ions $[Co(CN)_5]^{3-}$, $[Rh(CN)_5]^{3-}$ and $[Ir(CN)_5]^{3-}$ of square-pyramidal geometry, we have obtained the molecular orbitals levels schemes and charge and spin distributions. The unpaired electron in the HOMO is considerably delocalized towards the ligands, and the degree of delocalization increases in the order Co<Rh<Ir. The splitting of the "crystal field" levels is appreciably larger for the Rh and Ir complexes.

The analysis of the contributions to the calculated electric field gradients shows that V_{zz} is determined by contractions of the molecular wave functions around the metal. These contractions are achieved by small admixtures of "shallow core" p orbitals in the valence

molecular orbitals. This effect is amplified by the higher core values of $< r^{-3} >$, and increases in the order Co<Rh<Ir. The calculated value of V_{zz} for $[Ir(CN)_5]^{3-}$ compares well with the experimental value derived from EPR measurements.

A good accord between theoretical and experimentally-obtained magnetic hyperfine parameters A_{ISO} and A_{ANISO} was obtained for $[Co(CN)_5]^{3-}$. For $[Rh(CN)_5]^{3-}$, the small value computed for $A_\perp$ is consistent with the upper limit determined by EPR spectroscopy. For both complexes, the large second-order term $A_\perp^{(2)}$ is of the same order of magnitude, but opposite sign, to the first-order dipolar term $A_\perp^D$. This explains the small total values of $A_\perp$ found. On the other hand, the second-order term $A_{||}^{(2)}$ is almost negligible. We found a critical dependence of the Fermi (A_F) contribution on the angle Θ between the axial and equatorial CN ligands. This is a consequence of the (n+1)s→nd_{z^2} charge transfer which occurs as Θ is increased.

Figure Captions

Figure 1 - Square-pyramidal $[Co(CN)_5]^{3-}$; the complexes $[Rh(CN)_5]^{3-}$ and $[Ir(CN)_5]^{3-}$ have similar structures.

Figure 2 - Molecular orbitals energy levels of $[Co(CN)_5]^{3-}$, $[Rh(CN)_5]^{3-}$ and $[Ir(CN)_5]^{3-}$. Arrow denotes unpaired electron in HOMO.

Figure 3 - Populations of transition metal in HOMO for $[Co(CN)_5]^{3-}$ $(17a_1\uparrow)$, $[Rh(CN)_5]^{3-}$ $(20a_1\uparrow)$ and $[Ir(CN)_5]^{3-}$ $(24a_1\uparrow)$, for different values of Θ.

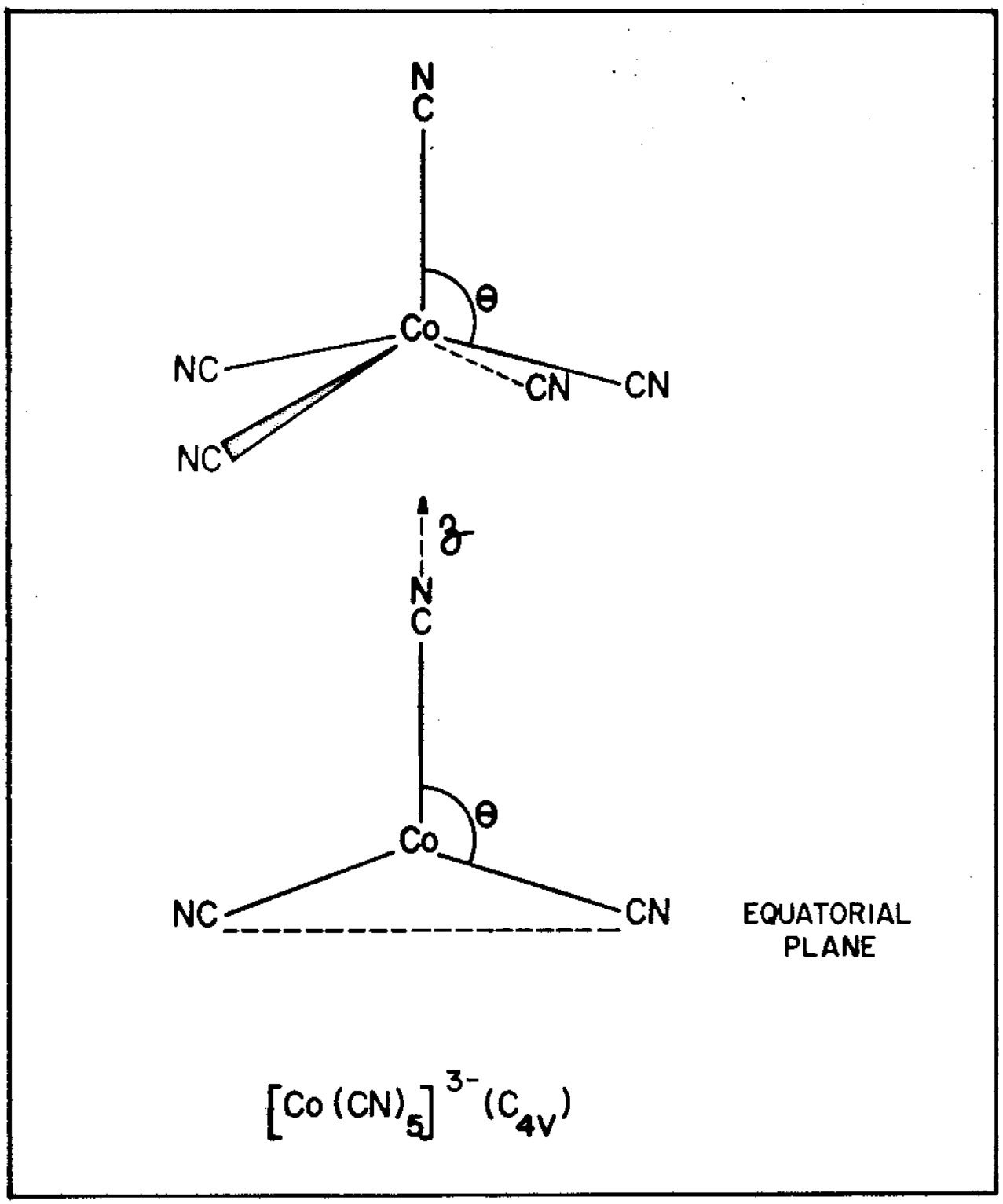

Fig. 1

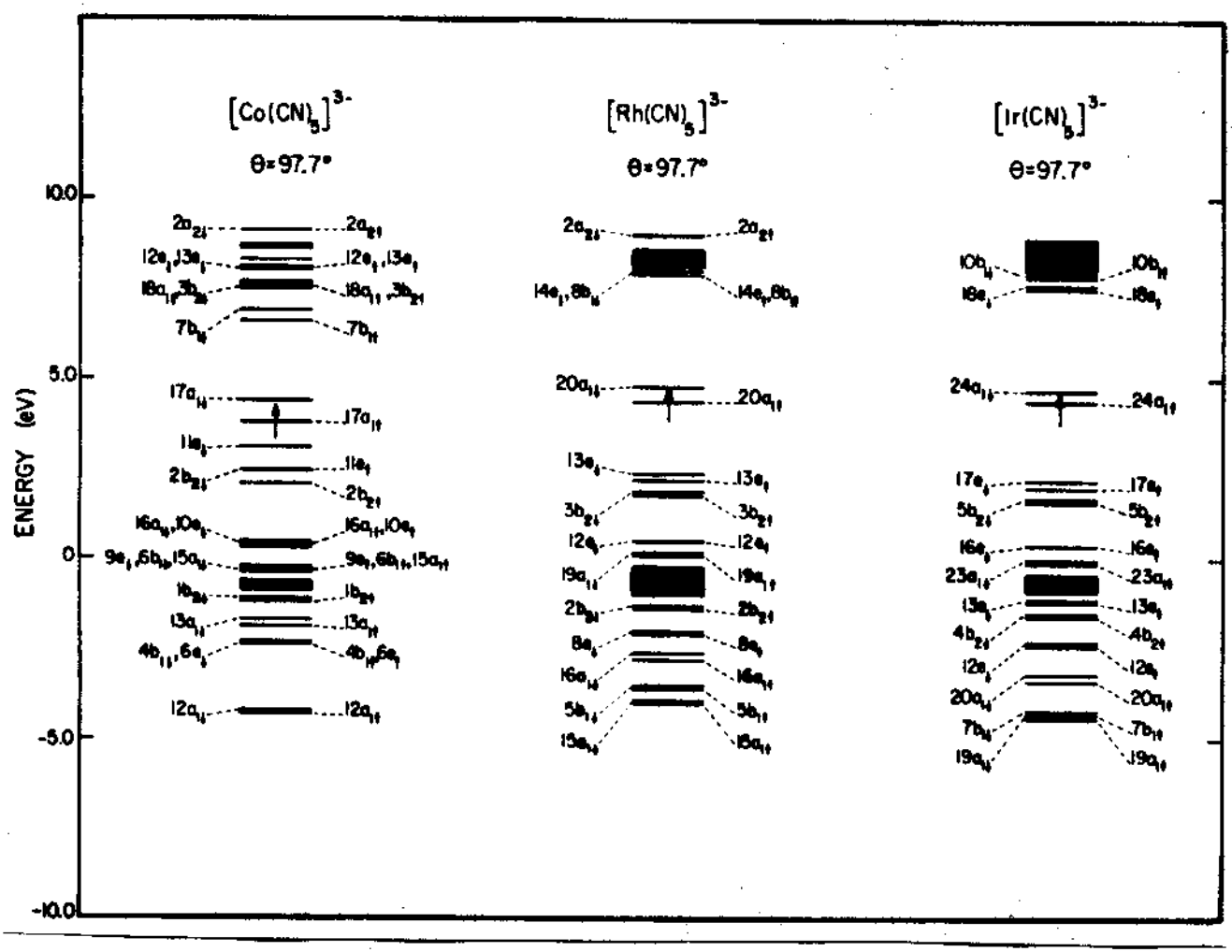

Fig. 2

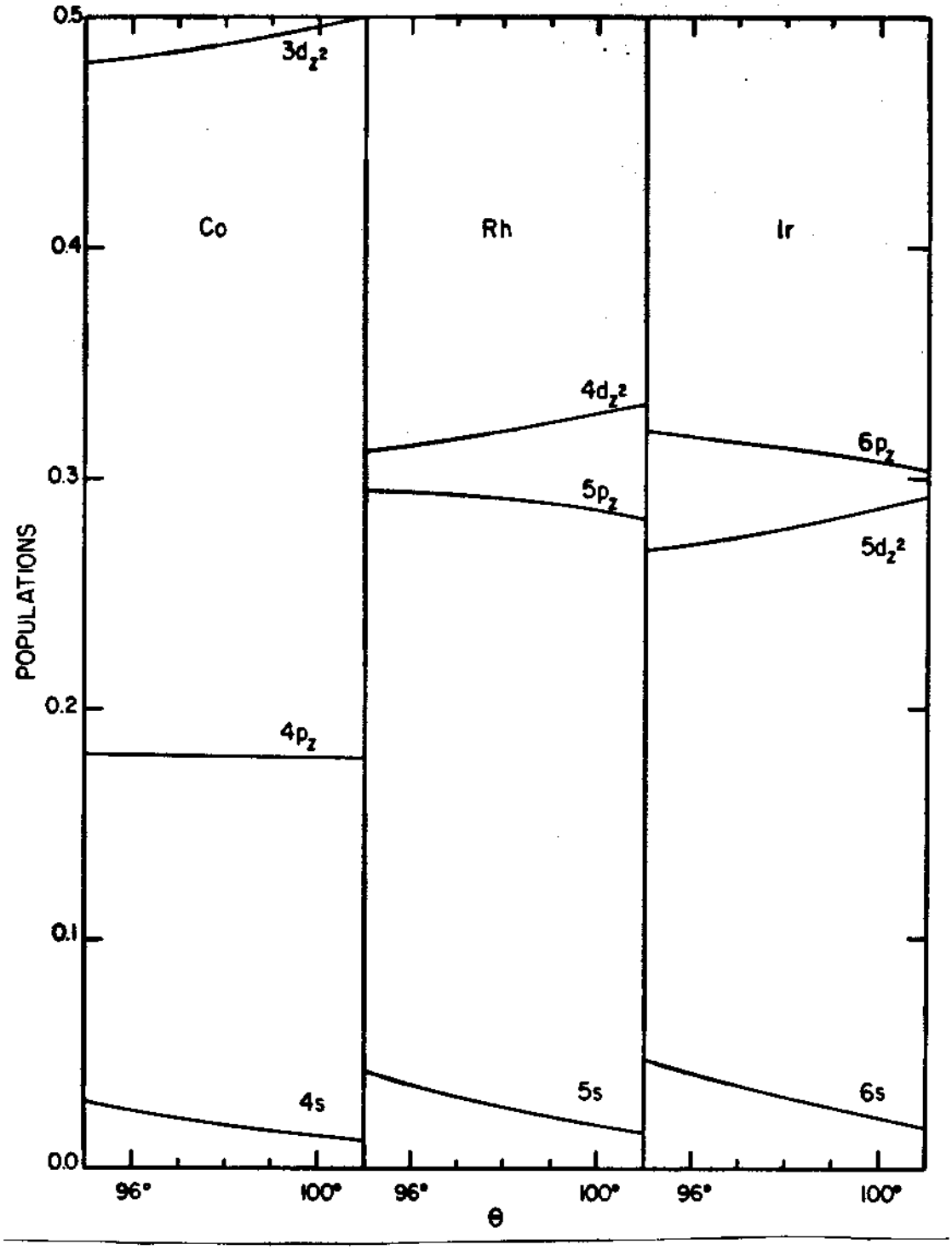
0.5
0.4
0.3
0.2
0.1
0.0
POPULATIONS
Co
Rh
Ir
3d$_{z^2}$
4p$_z$
4s
4d$_{z^2}$
5p$_z$
5s
6p$_z$
5d$_{z^2}$
6s
96°
100°
96°
100°
96°
100°
θ

Fig. 3

Table Captions

Table I -Populations, charges and magnetic moments of $[Co(CN)_5]^{3-}$, $[Rh(CN)_5]^{3-}$ and $[Ir(CN)_5]^{3-}$, for $\Theta = 97.7^0$.

Table II - Electric field gradients V_{zz} at the site of the transition metal for $[Co(CN)_5]^{3-}$, $[Rh(CN)_5]^{3-}$ and $[Ir(CN)_5]^{3-}$, for $\Theta = 97.7^0$.
a) From reference [23]; $Q(^{193}Ir)$=+0.78b [24].

Table III - Analysis by irreducible representations of the C_{4v} point group of the valence contribution to V_{zz}. Values in a_0^{-3}; $\Theta = 97.7^0$.

Table IV - Values of $< r^{-3} >$ calculated with atomic radial functions for Co, Rh and Ir, in $a_0^{-3(a)}$.
a) Atomic calculations performed for the configurations obtained for the complexes, at 97.7^0.

Table V - Values of the components of the hyperfine tensor $\tilde{A}$ at the Co site for $[Co(CN)_5]^{3-}$ (in $10^{-4}cm^{-1}$).
a) $g_N(^{59}Co)$=+1.326 [30].
b) From reference [25] (T=77K; dispersion is $\pm 2 \times 10^{-4}cm^{-1}$).
c) From reference [28]. T=77K.

Table VI - Contributions to $[\rho_\uparrow(0) - \rho_\downarrow(0)]$ at the transition metal nucleus for $[Co(CN)_5]^{3-}$ and $[Rh(CN)_5]^{3-}$, in a_0^{-3}; $\Theta = 97.7^0$.

Table VII - Values of the components of the magnetic hyperfine tensor $\tilde{A}$ at the Rh site for $[Rh(CN)_5]^{3-}$ (in $10^{-4}cm^{-1}$).
a) $g_N(^{103}Rh)$=−0.176 [30].
b) From reference [29].

Table I

	Populations on Metal					Charges						
	ns	np	nd	(n+1)s	(n+1)p	Metal	C_{ax}	C_{eq}	N_{ax}	N_{eq}	CN_{ax}	CN_{eq}
$[Co(CN)_5]^{3-}$	1.97	5.96	7.61	0.10	0.47	+0.89	+0.13	+0.11	-0.91	-0.89	-0.78	-0.78
$[Rh(CN)_5]^{3-}$	1.95	5.93	7.61	0.11	0.52	+0.88	+0.12	+0.09	-0.87	-0.88	-0.75	-0.78
$[Ir(CN)_5]^{3-}$	1.94	5.91	7.42	0.09	0.47	+1.17	+0.07	+0.02	-0.85	-0.87	-0.79	-0.84

	Magnetic Moments (μ_B)							
	Metal							
	nd	(n+1)s	(n+1)p	Total	C_{ax}	C_{eq}	N_{ax}	N_{eq}
$[Co(CN)_5]^{3-}$	0.72	0.02	0.11	0.85	0.10	0.0	-0.02	0.02
$[Rh(CN)_5]^{3-}$	0.44	0.03	0.18	0.65	0.15	0.02	-0.03	0.03
$[Ir(CN)_5]^{3-}$	0.39	0.03	0.20	0.62	0.13	0.03	-0.02	0.04

	Distribution of unpaired electron in HOMO							
	Metal							
	nd	(n+1)s	(n+1)p	Total	C_{ax}	C_{eq}	N_{ax}	N_{eq}
$[Co(CN)_5]^{3-}$	0.49	0.02	0.18	0.69	0.12	0.02	0.03	0.02
$[Rh(CN)_5]^{3-}$	0.32	0.03	0.29	0.64	0.10	0.03	0.03	0.02
$[Ir(CN)_5]^{3-}$	0.28	0.03	0.31	0.62	0.09	0.04	0.03	0.03

CBPF-NF-007/94

Table II

	Contributions to $V_{zz}(a_0^{-3})$			Total V_{zz}	Experimental[a]
	Shallow core	Valence	Nuclear	$(10^{17}\mathrm{V}/cm^2)$	$\lvert V_{zz}\rvert(10^{17}\mathrm{V}/cm^2)$
$[Co(CN)_5]^{3-}$	-0.06	+0.43	-0.35	+0.2	
$[Rh(CN)_5]^{3-}$	-0.27	+1.39	-0.26	+8.4	
$[Ir(CN)_5]^{3-}$	-0.60	+2.93	-0.26	+20.1	NaCl:|25.1|±0.3
					KCl:|21.3|±0.3
					RbCl:|13.0|±0.3

Table III

	$a_1(p_z,d_{z^2})$	$b_1(d_{x^2-y^2})$	$b_2(d_{xy})$	$e(p_{x,y},d_{xz,yz})$	Total Valence
$[Co(CN)_5]^{3-}$ (all electrons)	-5.04	+2.54	+5.73	-2.80	+0.43
$[Rh(CN)_5]^{3-}$ (all electrons)	-8.06	+3.03	+6.59	-0.17	+1.39
$[Ir(CN)_5]^{3-}$ (all eletrons)	-14.15	+4.76	+10.39	+1.93	+2.93
$[Co(CN)_5]^{3-}$ (frozen core)	-4.61	+2.57	+5.70	-3.68	-0.02
$[Rh(CN)_5]^{3-}$ (frozen core)	-6.23	+3.12	+6.57	-3.39	+0.07
$[Ir(CN)_5]^{3-}$ (frozen core)	-10.10	+4.88	+10.35	-5.03	+0.10

Table IV

	$< r^{-3} >_{np}$	$< r^{-3} >_{(n+1)p}$	$< r^{-3} >_{nd}$
Co	65.8	3.0	5.7
Rh	79.2	5.1	6.8
Ir	130.2	10.1	11.0

Table V

	Θ	A_F	$A_{\parallel}^D$	$A_{\perp}^D$	$A_{\parallel}^{(2)}$	$A_{\perp}^{(2)}$	$A_{\parallel}$	$A_{\perp}$	A_{ISO}	A_{ANISO}
Calculated[a]	95^0	+11.2	+109	-54.5	-5.3	+34.8	+114.9	-8.5	+32.6	+41.1
	97.7^0	-4.7	+110	-55.0	-5.5	+38.1	+99.8	-21.6	+18.9	+40.5
	101^0	-21.4	+110	-55.0	-6.2	+45.4	+82.4	-31.0	+6.8	+37.8
Experimental[b]								NaCl	+5.3	+37.1
								NaBr	+13.4	+35.8
								NaI	+14.3	+34.9
								KCl	+8.1	+38.0
								KBr	+14.3	+34.9
								KI	+12.8	+35.7
								KCN	+12.4	+35.8
								$K_3[Co(CN)_6]$	+11.4	+35.7
								Ethylene glicol-water solution[c]	+8.7	+37.0

CBPF-NF-007/94

Table VI

	$[Co(CN)_5]^{3-}$	$[Rh(CN)_5]^{3-}$
Core	-0.147	-0.142
$a_1\uparrow$(HOMO)	+0.110	+0.196
Total Valence	+0.134	+0.224
Total	-0.013	+0.082

Table VII

	Θ	A_F	$A_{\parallel}^D$	$A_{\perp}^D$	$A_{\parallel}^{(2)}$	$A_{\perp}^{(2)}$	$A_{\parallel}$	$A_{\perp}$	A_{ISO}	A_{ANISO}
Calculated[a]	95^0	-8.3	-19.3	+9.7	+2.3	-8.2	-25.3	-6.8	-13.0	-6.2
	97.7^0	-3.8	-19.4	+9.7	+2.3	-8.3	-20.9	-2.4	-8.6	-6.2
	101^0	+0.5	-19.5	+9.8	+1.8	-8.3	-17.2	+2.0	-4.4	-6.4
Experimental[b]							—	NaCl:< 5	—	—

References

[1] N.V. Vugman and V.K. Jain, Rev. Roumaine Phys. **33**, 981 (1988).

[2] A. Abragam and M.H.L. Pryce, Proc. Roy. Soc. **A205**, 135 (1951).

[3] A. Abragam, "The principles of nuclear magnetism", Oxford University Press, Oxford (1961).

[4] D.E. Ellis and G.S. Painter, Phys. Rev. **B2**, 2887 (1970); D.E. Ellis, Int. J. Quantum Chem. **S2**, 35 (1968); E.J. Baerends, D.E. Ellis and P. Ros, Chem. Phys. **2**, 41 (1973).

[5] R.G. Parr and W. Yang, "Density functional theory of atoms and molecules", Oxford University Press, N. York (1989).

[6] T. Ziegler, Chem. Rev. **91**, 651 (1991).

[7] W. Kohn and L.J. Sham, Phys. Rev. **140**, A1133 (1965).

[8] U. von Barth and L. Hedin, J. Phys. **C5**, 1629 (1972).

[9] B. Delley and D.E. Ellis, J. Chem. Phys. **76**, 1949 (1982).

[10] R.S. Mulliken, J. Chem. Phys. **23**, 1833 (1955).

[11] C. Umrigar and D.E. Ellis, Phys. Rev. **B21**, 852 (1980).

[12] A.H. Stroud, "Approximate calculation of multiple integrals", Prentice-Hall, N. Jersey (1971).

[13] N.V. Vugman, R.P.A. Muniz and J. Danon, J. Chem. Phys. **57**, 1297 (1972).

[14] L.D. Brown and K.N. Raymond, Inorg. Chem. **14**, 2590 (1975).

[15] F.A. Jurnak and K.N. Raymond, Inorg. Chem. **13**, 2387 (1974).

[16] J.J. Alexander and H.B. Gray, Coord. Chem. Rev. **2**, 29 (1967).

[17] J.C. Slater, "Quantum theory of molecules and solids", vol. 4, McGraw-Hill, N. York (1974).

[18] D. Guenzburger, A.O. Caride and E. Zuleta, Chem. Phys. Letters, **14**, 239 (1972).

[19] J.J. Alexander and H.B. Gray, J. Am. Chem. Soc. **90**, 4260 (1968).

[20] G.L. Geoffroy, M.S. Wrighton, G.S. Hammond and H.B. Gray, Inorg. Chem. **13**, 430 (1974).

[21] D.E. Ellis, D. Guenzburger and H.B. Jansen, Phys. Rev. **B28**, 3697 (1983).

[22] P. Gütlich, R. Link and A. Trautwein, "Mössbauer spectroscopy and transition metal chemistry", Springer-Verlag, Berlin (1978); N.N. Greenwood and T.C. Gibb, "Mössbauer spectroscopy", Chapman and Hall, London (1971).

[23] N.M. Pinhal and N.V. Vugman, Hyperfine Int. **52**, 89 (1989).

[24] "Table of Isotopes", edit. C.M. Lederer and V.S. Shirley, 7^{th} edition, John Wiley, N. York (1980).

[25] M.C.R. Symons and J.G. Wilkinson, J. Chem. Soc. (A), 2069 (1971).

[26] D. Guenzburger and D.E. Ellis, Phys. Rev. **B22**, 4203 (1980).

[27] S.R. Nogueira and D. Guenzburger, Phys. Rev. **A44**, 5558 (1991).

[28] F.-D. Tsay, H.B. Gray and J. Danon, J. Chem. Phys. **54**, 3760 (1971).

[29] N.V. Vugman, private communication.

[30] B.A. Goodman and J.B. Raynor, J. Inorg. Nuclear Chem. **32**, 3406 (1970).